Astrodynamics Vol. 2, No. 3, 217–231, 2018 https://doi.org/10.1007/s42064-018-0022-0

Angles-only initial relative orbit determination algorithm for non-cooperative spacecraft proximity operations

Baichun Gong[1], Wendan Li[1], Shuang Li[1](✉), Weihua Ma[2], and Lili Zheng[3]

1. Advanced Space Technology, Nanjing University of Aeronautics and Astronautics, Nanjing210016, China
2. National Key Laboratory of Aerospace Flight Dynamics, Northwestern Polytechnical University, Xi'an 710072, China
3. Beijing Institute of Aerospace System Engineering, Beijing 100076, China

ABSTRACT

This research furthers the development of a closed-form solution to the angles-only initial relative orbit determination problem for non-cooperative target close-in proximity operations when the camera offset from the vehicle center-of-mass allows for range observability. In previous work, the solution to this problem had been shown to be non-global optimal in the sense of least square and had only been discussed in the context of Clohessy–Wiltshire. In this paper, the emphasis is placed on developing a more compact and improved solution to the problem by using state augmentation least square method in the context of the Clohessy–Wiltshire and Tschauner–Hempel dynamics, derivation of corresponding error covariance, and performance analysis for typical rendezvous missions. A two-body Monte Carlo simulation system is used to evaluate the performance of the solution. The sensitivity of the solution accuracy to camera offset, observation period, and the number of observations are presented and discussed.

KEYWORDS

initial relative orbit determination
angles-only navigation
proximity operations
rendezvous

Research Article

Received: 20 November 2017
Accepted: 28 January 2018

1 Introduction

Relative navigation is one of the key enable technologies of on-orbit servicing for space non-cooperative target [1]. The angles-only relative navigation based on passive optical camera is suitable for non-cooperative target's mission due to its simplicity and reliability. The projects PRISMA [2] already have done on-orbit experiments to test the feasibility of angles-only relative navigation for non-cooperative target. The projects DEOS [3] and Phoenix [4] are also planned to develop angles-only relative navigation technique for non-cooperative targets, such as disabled satellite and space debris. However, the angles-only problem suffers from a range observability problem during near-range rendezvous, especially co-planar rendezvous. Woffinden and Geller [5] elegantly show that the angles-only relative navigation during orbital proximity operations is not observable if the chaser and target are in free motion and the motion is modeled by the linearized Clohessy–Wiltshire (CW) equations.

To overcome the range observability problem, a lot of work has to be done. Woffinden and Geller [6] proposed the orbital maneuver method to improve observability. Li *et al.* [7] expanded the strategies of orbital maneuver for observability's improvement. Grzymisch and Ficher [8] analyzed the observability from another perspective and provided several classical unobservable maneuver set. Luo *et al.* [9] studied the problem from the frame of closed-loop guidance based on multi-pulse sliding guidance strategy. Jagat and Sinclair [10] proposed an information-weighted LQG maneuver approach for angles-only relative navigation. Gaias *et al.* [1] investigated this topic from the point of the relative orbit elements. Newman *et al.* [11, 12] successfully applied second-order relative motion models to obtain observability. Sullivan *et al.* [13] utilized an improved J2-perturbed dynamic model and nonlinear measurement model to demonstrate the feasibility of maneuver-free angles-only navigation. Gasbarri *et al.* [14] took advantage of prior information of the target (i.e.,

✉ lishuang@nuaa.edu.cn

Nomenclature

IROD	Initial relative orbit determination
LVLH	Local vertical local horizon
$\hat{r}_0$,$\hat{v}_0$	Initial relative position and velocity solution
ω	Angular rate of the chaser orbit (rad/s)
$\phi_{rr}(i), \phi_{rv}(i), \phi_{vr}(i)$, and $\phi_{vv}(i)$	3×3 partitions of the state transition matrix
$\boldsymbol{i}_{\text{los}}(i)$	Line-of-sight in LVLH frame
$\boldsymbol{d}^c$	Camera position in chaser body frame (m)
$\boldsymbol{b}_d$	Camera installation bias (m)
ε_i	Camera measurement noise
σ_{cam}	Standard deviation of camera measurement noise
$\boldsymbol{b}_\xi$	Attitude bias
$\nu(i)$	Attitude measurement noise
σ_{att}	Standard deviation of attitude measurement noise
$\boldsymbol{M}$	IROD estimate error mean
P	IROD estimate error covariance
N	Number of observations
$T^{\text{lvlh}}_{\text{chaser}}$	Direction cosine matrix from chaser body frame to LVLH frame
n	Monte Carlo runs
M_ρ	Range estimate error mean from Monte Carlo simulations
σ_ρ	Range estimate error standard deviation from Monte Carlo simulations
R_{C}	Radius of the chaser orbit

a reference image of the target) to overcome the problem. Chen and Xu [15] presented a double line-of-sight measuring scheme to obtain observability while two spacecraft (cameras) were utilized. Gao *et al.* [16] proposed a distributed angles-only navigation method based on multiple line-of-sights.

Recently, a new solution to the angles-only problem was demonstrated which does not require orbital maneuvers, high-order dynamics, a priori knowledge of target geometry or a second camera. This solution requires only an optical camera offset from the chaser center-of-mass with or without rotational maneuvers [17, 18]. The solution to the angles-only initial relative orbit determination (IROD) problem for close-in orbital proximity operations was developed by Geller and Perez [19]. The performance of the solution was analyzed by Gong and Geller [20]. However, the result has shown that the solution is not optimal in the sense of least square,(i.e., more observations do not always mean a smaller covariance). Additionally, the performance of the solution has only been demonstrated in the context of the CW equations.

The objective of this paper is to develop a global optimal least square algorithm for the angles-only IROD problem with different accurate dynamics for space non-cooperative target during close-in proximity operations, while camera offset provides observability, obtaining the explicit estimation error covariance expression with respect to camera offsetand evaluating the performance for typical rendezvous missions. The relative motion dynamics and observation model for the IROD algorithms are set up in Section 2, the general solution based on state augmentation least square method and its analytic estimate error covariance with the consideration of sensors uncertainties are presented in Section 3. Monte Carlo simulations including two-bodydynamics, reference mission and trajectories, key parameters setting and performance analysis are presented in Section 4. Conclusions are presented in Section 5.

2 Relative motion dynamics and observation model

2.1 Relative motion dynamics

Under the assumption of the two body problems and the distance between the chaser and target is small compared to the distance of the target to the center of the Earth, the relative motion dynamics during coasting flight that is applicable to eccentric orbit can be given in the chaser-orbital Local vertical local horizontal (LVLH) frame as the following [21]:

$$\begin{aligned} \ddot{x} - 2\omega\dot{z} - \omega^2 x - \dot{\omega} z + \tfrac{\mu}{R_{\text{C}}^3} x = 0 \\ \ddot{y} + \tfrac{\mu}{R_{\text{C}}^3} y = 0 \\ \ddot{z} + 2\omega\dot{x} - \omega^2 z + \dot{\omega} x - \tfrac{2\mu}{R_{\text{C}}^3} z = 0 \end{aligned} \tag{1}$$

where z axis points in the nadir direction, y axis is normal to the orbital plane, opposite the angular

momentum vector, and x axis completes the right-hand system, ω is the angular rate of the chaser orbit. Moreover, μ is the gravitational parameter and R_{C} is the radius of the chaser orbit.

Equation (1) can be analytically solved by being transformed into Tschauner–Hempel (TH) Ref. [21] as follows:

$$\begin{aligned} \tilde{x}'' &= 2\tilde{z}' \\ \tilde{y}'' &= -\tilde{y} \\ \tilde{z}'' &= 3\tilde{z}/\lambda - 2\tilde{z}' \end{aligned} \tag{2}$$

where $\tilde{x}$, $\tilde{y}$ and $\tilde{z}$ are dependent-variable of true anomaly θ and relative orbit, $()' = \mathrm{d}()/\mathrm{d}\theta$, $()'' = \mathrm{d}^2()/\mathrm{d}\theta^2$. More details could be found in Ref. [21]:

Then the state transition matrix could be obtained in the sense of true anomaly for elliptic orbit [22]. If the orbit is near-circular, Eq. (1) can be reduced to the renowned Clohessy–Wiltshire equations, which also has analytic solution [23]. Thus, the relative state can be propagated by the following equations:

$$\begin{bmatrix} \boldsymbol{r}(i) \\ \boldsymbol{v}(i) \end{bmatrix} = \begin{bmatrix} \phi_{rr}(i) & \phi_{rv}(i) \\ \phi_{vr}(i) & \phi_{vv}(i) \end{bmatrix} \begin{bmatrix} \boldsymbol{r}(0) \\ \boldsymbol{v}(0) \end{bmatrix} \tag{3}$$

where $\boldsymbol{r}(0)$, $\boldsymbol{v}(0)$ are the position and velocity at $t = 0$, $\boldsymbol{r}(i)$, $\boldsymbol{v}(i)$ are the position and velocity at time t_i, and the state transition matrix partitions $\phi_{rr}(i)$, $\phi_{rv}(i)$, $\phi_{vr}(i)$ and $\phi_{vv}(i)$ are functions of time for near-circular orbit case or true anomaly for elliptic orbit case.

2.2 Observation model

Figure 1 illustrates the observation geometry associated with the camera offset angles-only navigation problem. It is assumed that the origin of the chaser body-fixed reference frame is co-located with the chaser center-of-mass. Without loss of generality it is also assumed that a camera is mounted on the body at a distance d from the chaser center-of-mass. The camera measurement frame is assumed to be aligned with the focal-plane of the camera, and its orientation with respect to the chaser body frame is supposed to be known and constant.

The pixel center location of the target image is used to form a line-of-sight (LOS) vector from camera to target center-of-mass. LOS observation can be expressed in the camera frame at time t_i by

$$\boldsymbol{i}_{\mathrm{los}}^{\mathrm{cam}}(i) = \frac{T_{\mathrm{lvlh}}^{\mathrm{cam}}(i)\boldsymbol{r}(i) - T_{\mathrm{chaser}}^{\mathrm{cam}}(i)\boldsymbol{d}^c}{\left\| T_{\mathrm{lvlh}}^{\mathrm{cam}}(i)\boldsymbol{r}(i) - T_{\mathrm{chaser}}^{\mathrm{cam}}(i)\boldsymbol{d}^c \right\|} \tag{4}$$

where $\boldsymbol{d}^c$ is the constant position of camera in chaser body frame. Since the transformation matrix from LVLH to the camera measurement frame $T_{\mathrm{lvlh}}^{\mathrm{cam}}(i)$ at time t_i is assumed to be known (using knowledge of inertial attitude, position, and velocity), an alternative description of the LOS measurement expressed in the LVLH frame, $\boldsymbol{i}_{\mathrm{los}}(i)$, can be utilized:

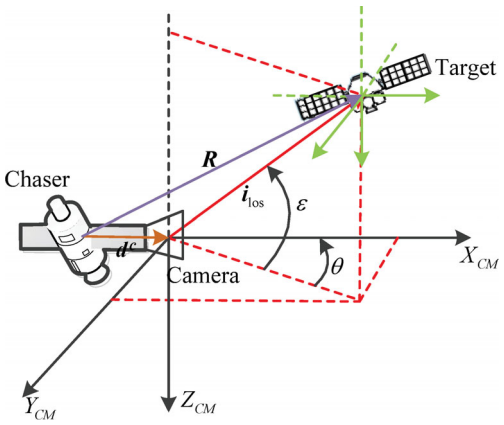

Fig. 1 Measurement frame and geometry.

$$\boldsymbol{i}_{\mathrm{los}}(i) = \frac{\boldsymbol{r}(i) - T_{\mathrm{chaser}}^{\mathrm{lvlh}}(i)\boldsymbol{d}^c}{\left\| \boldsymbol{r}(i) - T_{\mathrm{chaser}}^{\mathrm{lvlh}}(i)\boldsymbol{d}^c \right\|} \tag{5}$$

where the expression of $\boldsymbol{r}(i)$ can be propagated by the state transition matrix and the initial relative position and velocity $\boldsymbol{r}(0)$ and $\boldsymbol{v}(0)$. Thus, the LOS time-history in the LVLH frame also can be determined by Eq. (5) but with a different state transition matrix based on CW dynamics and TH dynamics, respectively.

3 IROD solution and covariance based on state augmentation least square

3.1 IROD solution based on state augmentation least square

When the camera offset is not equal to zero, it has been shown that the angles-only relative orbit determination problem might be observable [18] and an alternative solution to the IROD problem has been presented [19]. However, the solution of this prototype algorithm is not global optimal in the sense of least square that more observations do not always mean smaller covariance [20]. The reason for this problem is that initial relative state and scale factors were solved separately, where the least square approach was designed to minimize the estimate error of the scale factors but not the initial relative state. Further, it can be found that actually only the first two LOS measurements were used to

calculate initial relative state after the scale factors were obtained. As a result, the prototype algorithm does not make full use of the available observations. Thus, in order to overcome the existing problem as being analyzed, an improved least square solution for the IROD problem by means of state augmentation is proposed, where the scale factors and the initial relative state will be solved together.

As the initial relative state is a 6-dimension variable and only two LOS angles are available on each epoch, at least three sets of LOS angles should be obtained to solve the state. Assume there have $N \geqslant 3$ set of observations and consider the first LOS observation, $\boldsymbol{i}_{\text{los}}(0)$. The solution for the initial position $\boldsymbol{r}(0)$ must satisfy:

$$k_0 \boldsymbol{i}_{\text{los}}(0) = \boldsymbol{r}(0) + T^{\text{lvlh}}_{\text{chaser}}(0)\boldsymbol{d}^c \tag{6}$$

where k_0 is the unknown scale factor of $\boldsymbol{i}_{\text{los}}(0)$. Similarly, for the second observation the corresponding the IROD solution $\hat{\boldsymbol{r}}(0)$, $\hat{\boldsymbol{v}}(0)$ must satisfy:

$$k_1 \boldsymbol{i}_{\text{los}}(1) = \phi_{rr}(1)\boldsymbol{r}(0) + \phi_{rv}(1)\boldsymbol{v}(0) + T^{\text{lvlh}}_{\text{chaser}}(1)\boldsymbol{d}^c \tag{7}$$

where k_1 is also unknown scale factor of $\boldsymbol{i}_{\text{los}}(1)$. And the i^{th} observation must satisfy:

$$k_i \boldsymbol{i}_{\text{los}}(i) = \phi_{rr}(i)\boldsymbol{r}(0) + \phi_{rv}(i)\boldsymbol{v}(0) + T^{\text{lvlh}}_{\text{chaser}}(i)\boldsymbol{d}^c \tag{8}$$

Thus, here $3N$ equations with $(N+6)$ unknowns can be obtained from N sets of LOS angles. As being analyzed in the beginning of this section, the scale factors and the initial relative state are combined as an augmentation estimate state, i.e., $\boldsymbol{X} = [k_0, \cdots, k_{N-1}, \boldsymbol{r}(0)^{\text{T}}, \boldsymbol{v}(0)^{\text{T}}]^{\text{T}}$. Then, rearranging the equations into matrix form yields:

$$\boldsymbol{A}_N \boldsymbol{X}_N = \boldsymbol{B}_N \tag{9}$$

where

$$\boldsymbol{A}_N = \begin{bmatrix} \boldsymbol{i}_{\text{los}}(0) & 0 & 0 & 0 & -I & 0 \\ 0 & \boldsymbol{i}_{\text{los}}(1) & 0 & 0 & -\phi_{rr}(1) & -\phi_{rv}(1) \\ & & \ddots & & \vdots & \vdots \\ 0 & 0 & & 0 & \vdots & \vdots \\ 0 & 0 & 0 & \boldsymbol{i}_{\text{los}}(N-1) & -\phi_{rr}(N-1) & -\phi_{rv}(N-1) \end{bmatrix} \tag{10}$$

$$\boldsymbol{B}_N = \begin{bmatrix} T^{\text{lvlh}}_{\text{chaser}}(0) \\ T^{\text{lvlh}}_{\text{chaser}}(1) \\ \vdots \\ T^{\text{lvlh}}_{\text{chaser}}(N-1) \end{bmatrix} \tag{11}$$

Then, a least-square solution to this set of over-determined equations can be obtained from where the IROD solution would be abstracted as follows:

$$\hat{x}_0 = \begin{bmatrix} \hat{r}_0 \\ \hat{v}_0 \end{bmatrix} = \boldsymbol{C}_N \hat{\boldsymbol{X}}_N = \boldsymbol{C}_N (\boldsymbol{A}_N^{\text{T}} \boldsymbol{A}_N)^{-1} \boldsymbol{A}_N^{\text{T}} \boldsymbol{B}_N \tag{12}$$

where

$$\boldsymbol{C}_N = [\boldsymbol{0}_{6\times N} \quad \boldsymbol{I}_{6\times 6}] \tag{13}$$

and when only three observations are available, the pseudo-inverse term $(\boldsymbol{A}_N^{rmT}\boldsymbol{A}_N)^{-1}\boldsymbol{A}_N^{rmT}$ will reduce to $\boldsymbol{A}_N^{-1}$.

Thus, Eq. (12) represents a simple algorithm that can be used to determine the IROD solution for any relative motion coasting trajectory, and for any known constant or time-varying chaser orientation.

Additionally, the solution shown in Eq. (12) could achieve better performance than the prototype algorithm when more observations are available. But two solutions would be equivalent if there are only three observations, which will be depicted by digital simulations in Section 4.

3.2 Estimate error covariance

The IROD algorithm requires knowledge of $\boldsymbol{d}^c$, $\boldsymbol{i}_{rmlos}(i)$ and $T^{\text{lvlh}}_{\text{chaser}}(i)$. The measured values of these variables $\tilde{\boldsymbol{d}}^c$, $\tilde{\boldsymbol{i}}_{\text{los}}(i)$ and $\tilde{T}^{\text{lvlh}}_{\text{chaser}}(i)$ contain errors which will lead to estimation errors in the initial relative orbit. Thus, error models for these variables are required.

The camera offset $\boldsymbol{d}^c$ is assumed to contain a fixed error $\boldsymbol{b}_d$ which is modeled as a constant. And the chaser's attitude error $\xi(i)$ is assumed to be small and modeled as an constant bias $\boldsymbol{b}_\xi$ with a zero mean Gaussian white noise $\upsilon(i)$ whose standard deviation is σ_{att}. Moreover, the LOS observation $\tilde{\boldsymbol{i}}_{\text{los}}(i)$ is supposed to be perturbed by a zero mean Gaussian noise ε_i with a standard deviation σ_{cam}.

Then, covariance analysis can be conducted based on statistical theory [20]. By substituting the contaminated observations with bias and random noise from sensors into the solution shown in Eq. (12), the expression for estimate error could be obtained. Then, by calculating first and second order moment, the explicit expressions of analytic estimate error mean and covariance with respect to camera offset could be derived as follows:

$$\boldsymbol{M} = \boldsymbol{H}_1 \boldsymbol{b}_d - \boldsymbol{C}_N \boldsymbol{A}_N^{+-1} \begin{bmatrix} T^{\text{lvlh}}_{\text{chaser}}(0) \\ \vdots \\ T^{\text{lvlh}}_{\text{chaser}}(N-1) \end{bmatrix} [\boldsymbol{b}_\xi \times] \boldsymbol{d}^c \tag{14}$$

$$\boldsymbol{P}=\sigma_{\mathrm{cam}}^{2}\boldsymbol{H}_{2}\boldsymbol{\Lambda}\boldsymbol{H}_{2}^{\mathrm{T}}+\sigma_{\mathrm{att}}^{2}\boldsymbol{C}_{N}\boldsymbol{A}_{N}^{+-1}\begin{bmatrix}\lambda_{0}(\boldsymbol{d}^{c}) & & \\ & \ddots & \\ & & \lambda_{N-1}(\boldsymbol{d}^{c})\end{bmatrix}\boldsymbol{A}_{N}^{+-\mathrm{T}}\boldsymbol{C}_{N}^{\mathrm{T}} \tag{15}$$

where $\boldsymbol{H}_{1}=\boldsymbol{C}_{N}\boldsymbol{A}_{N}^{+-1}\boldsymbol{H}_{B_d}$, $\boldsymbol{H}_{2}=\boldsymbol{C}_{N}\boldsymbol{A}_{N}^{+-1}\boldsymbol{H}_{A}$, $\boldsymbol{A}_{N}^{+-1}=\left(\boldsymbol{A}_{N}^{\mathrm{T}}\boldsymbol{A}_{N}\right)^{-1}\boldsymbol{A}_{N}^{\mathrm{T}}$, $\lambda_{i}(\boldsymbol{d}^{c})$ is a function of camera offset and time:

$$\lambda_{i}(\boldsymbol{d}^{c})=T_{\mathrm{chaser}}^{\mathrm{lvlh}}(i)\left[\boldsymbol{d}^{c}\times\right]\left[\boldsymbol{d}^{c}\times\right]^{\mathrm{T}}T_{\mathrm{chaser}}^{\mathrm{lvlh}}(i)^{\mathrm{T}} \tag{16}$$

The expressions for $\boldsymbol{\Lambda}$, $\boldsymbol{H}_{A}$ and $\boldsymbol{H}_{B_d}$ are as follows:

$$\boldsymbol{\Lambda}=\begin{bmatrix}k_{0}^{2}\boldsymbol{I}_{3\times3} & 0_{3\times3} & 0_{3\times3} & 0_{3\times3} & 0_{3\times3}\\ 0_{3\times3} & \ddots & 0_{3\times3} & 0_{3\times3} & 0_{3\times3}\\ 0_{3\times3} & 0_{3\times3} & k_{N-1}^{2}\boldsymbol{I}_{3\times3} & \vdots & \vdots\\ 0_{3\times3} & \cdots & 0_{3\times3} & 0_{3\times3} & 0_{3\times3}\\ 0_{3\times3} & \cdots & 0_{3\times3} & 0_{3\times3} & 0_{3\times3}\end{bmatrix} \tag{17}$$

$$\boldsymbol{H}_{A}=\begin{bmatrix}[\boldsymbol{i}_{\mathrm{los}}(0)\times] & 0_{3\times3} & 0_{3\times3} & 0_{3\times3} & 0_{3\times3} & 0_{3\times3}\\ 0_{3\times3} & [\boldsymbol{i}_{\mathrm{los}}(1)\times] & \ddots & \ddots & 0_{3\times3} & 0_{3\times3}\\ \vdots & \ddots & \ddots & 0_{3\times3} & \vdots & \vdots\\ 0_{3\times3} & \cdots & 0_{3\times3} & [\boldsymbol{i}_{\mathrm{los}}(N-1)\times] & 0_{3\times3} & 0_{3\times3}\end{bmatrix} \tag{18}$$

$$\boldsymbol{H}_{B_d}=\begin{bmatrix}T_{\mathrm{chaser}}^{\mathrm{lvlh}}(0)\\ \vdots\\ T_{\mathrm{chaser}}^{\mathrm{lvlh}}(N-1)\end{bmatrix} \tag{19}$$

It can be seen that the estimate error mean is linear related to the camera offset while the covariance is related to the second order of the camera offset.

4 Monte Carlo simulations

In this section the performance of the IROD algorithm will be presented as a function of key parameters. The material in this section will be divided into five parts. Firstly, the simulation models and reference missions will be described. Secondly, the key parameters are set up. Next, the influence of the camera offset and observation period on IROD performance will be examined. Lastly, IROD performance based on different dynamics will be examined and compared with that from prototype algorithm shown in Ref. [19].

4.1 Simulation models and reference missions

A standard Monte Carlo simulation was created using MATLAB to model the dynamics of the rendezvous scenarios to evaluate the performance of the proposed IROD algorithms in a two-body dynamics environment. The truth motion models include the chaser and target spacecraft orbital dynamics defined in the earth-centered inertial frame (x axis points toward the mean of the vernal equinox in the equatorial plane, z axis is normal to the equatorial plane and pointing north, y axis completes the orthogonal set). The state vector of the model is a 12-dimensional vector defined by the inertial position and velocity of the chaser and target $\boldsymbol{X}=[\boldsymbol{R}_{c};\boldsymbol{V}_{c};\boldsymbol{R}_{t};\boldsymbol{V}_{t}]$, then the dynamics equations for the true state vector are

$$\begin{aligned}\dot{\boldsymbol{R}}_{c}&=\boldsymbol{V}_{c}, & \dot{\boldsymbol{R}}_{t}&=\boldsymbol{V}_{t}\\ \dot{\boldsymbol{V}}_{c}&=\boldsymbol{g}_{c}(\boldsymbol{R}_{c}), & \dot{\boldsymbol{V}}_{t}&=\boldsymbol{g}_{t}(\boldsymbol{R}_{t})\end{aligned} \tag{20}$$

where $\boldsymbol{g}_{c}$ and $\boldsymbol{g}_{t}$ are the accelerations due to gravity acting on the chaser and target spacecraft respectively which are based on a point-mass gravity models [24]. Since the goal of the current analysis is to develop general first-order understanding of IROD performance and the accuracy of the analytic statistics, the effects of J_2 (and different orbit inclinations) and aerodynamic drag (and other vehicle dependencies) are not considered, as well as third body and other perturbations effects.

Next, it is assumed that both spacecraft are orbiting in low-Earth near-circular orbit. The target's initial orbit elements are as follows: semimajor axis, 6790.1 km; eccentricity, 0.001; inclination, 51.6455 deg; ascending node, 281.6522 deg; argument of perigee, 37.3945 deg; true anomaly, 322.7645 deg. The chaser is orbiting nearby to the target and keeping a fixed orientation with respect to LVLH frame, i.e., the chaser has no rotational motion with respect to LVLH. Moreover, both spacecraft are assumed to be in coasting flight.

Then, five different natural motion trajectories for proximity operations are considered to verify and test the proposed algorithm: V-bar station-keeping, Football, Oscillating, Co-elliptic and Hopping orbits. More detailed information about these trajectories can be found in Ref. [25]. Moreover, chaser's initial inertial position and velocity are determined by target's initial position and velocity plus the relative position and velocity associated with the particular natural motion relative trajectory.

Lastly, as the key of angles-only problem is to solve the range observability, the IROD performance will be measured by the range estimate accuracy based on Monte Carlo simulations. The range estimate error mean and its standard deviation are defined as the following:

$$\begin{aligned} M_\rho &= \delta\bar{e} = \frac{1}{n}\sum_{i=1}^{n}\delta e(i) = \frac{1}{n}\sum_{i=1}^{n}[\hat{\rho}(i)-\rho(i)], \\ \sigma_\rho &= \sqrt{\frac{1}{n-1}\sum_{i=1}^{n}[\delta e(i)-M_\rho]^2} \end{aligned} \tag{21}$$

where n is the number of Monte Carlo runs, $\hat{\rho}$ is the estimate of the relative range, ρ is the true relative range.

4.2 Key parameters setting

The nominal initial chaser position is 1000 m downrange of the target in +V-bar direction for V-bar stationary, Football, Oscillating, and Hopping orbits, while Co-elliptic orbit has an additional 100 m in initial relative altitude. The Hopping and Oscillating orbits have a maximum relative displacement of 100 m in the altitude and cross-track directions, respectively. The integration time-step is 10 s, the number of LOS observations varies from 3 to 13, and the total simulation time T_f will be differently set for the corresponding simulation cases in the following subsections. And all the simulations contain 200 Monte Carlo runs which roughly lead to a 90% confidence [26]. Additionally, the camera offset is assumed to be nominally in the out-of-plane direction, as an in-plane offset leads to poor range observability [18]. The more detailed settings for camera offset will be described in the following corresponding subsections. Moreover, Key parameters for sensors are provided in Table 1.

Table 1 Key parameters for sensors

Sensor \ Parameters	Bias	Random noise std
Camera	$\boldsymbol{b}_d = 1\%\boldsymbol{d}^c$	$\sigma_{\text{cam}} = 10^{-4}$rad
Attitude sensor	$\xi_d = 10^{-3}$rad/axis	$\sigma_{\text{att}} = 10^{-3}$rad/axis

4.3 Influence of camera offset

In order to verify the analytic expressions of the effect on camera offset shown in Eqs. (14) and (15), Monte Carlo simulations with the camera offset varying from 1 m to 10 m have been done.

Figure 2 shows how larger camera offset clearly improves IROD performance for a V-bar station-keeping trajectory when the initial chaser/target separation is 1000 m, $T_f = 6000$ s. As shown in the left figure, the error mean curves start to perform linearly as expressed in Eq. (14) after the camera offset larger than 2 m. The reason for the nonlinearity is that when the camera offset is not big enough with respect to the separation of two spacecrafts, it will not get sufficient observability for the estimation. As to elaborate this problem, another simulation with a smaller separation has been done as the following.

Figure 3 shows the results for 100 m initial separation. As we can see, the estimate error mean shows linearity with the increasing of camera offset which does coincide with the description of Eq. (14). Moreover, both of the right figures obviously indicate the second

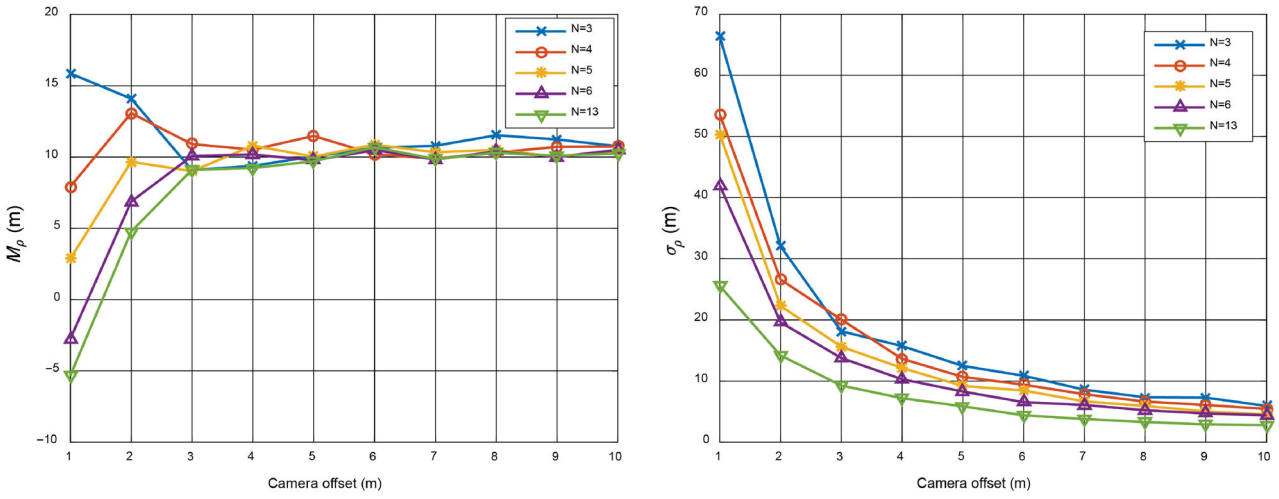

Fig. 2 Estimation error mean and standard deviation, $R_0 \approx 1000$ m.

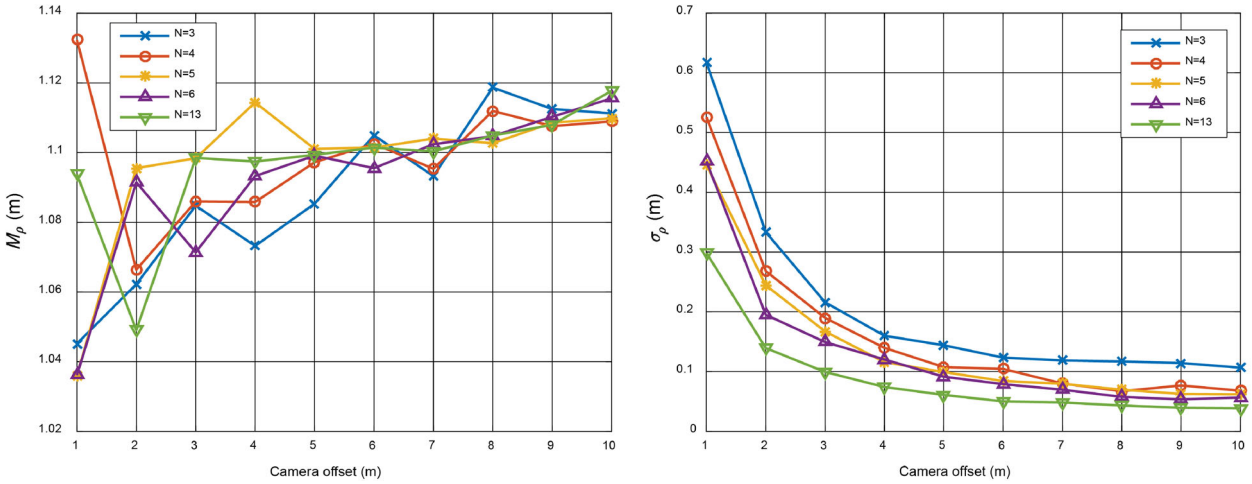

Fig. 3 Estimation error mean and standard deviation, $R_0 \approx 100$ m.

order relationship between camera offset and error covariance. And this relationship is independent of the separation distance.

Actually, the same conclusions can be made for other trajectories and the case when TH dynamics was considered.

4.4 Influence of observation period

It can be seen from subsection 3.2, the estimate error mean and covariance expressions are related to the observation period Δt by means of transition matrix, where Δt means the time interval between adjacent measurements. But it is pretty hard to derive the explicit expressions for error covariance about the observation period, because of the complexity of the transition matrix. As a result, two different kinds of simulation have been done to analyze the influence of the observation period on IROD performance. Case 1 fixed the observation number while the period increased which would lead a larger final time $T_f = N\Delta t$, and Case 2 fixed the final time whilst the observation periods decreased. In these simulations, the initial relative distance is about 1000 m when the camera offset is 1 m along cross-track with 1% uncertainties in three axes and the camera accuracy is in 10^{-4} rad level.

Figure 4 shows the results for Case 1 with an increasing final time. It can be seen that the estimate error mean and standard deviation generally converge as Δt increases, no matter what kind of dynamics is used or how many observations are utilized. However, when Δt is too small, for example smaller than 700, the estimate error and covariance are pretty large which means fake solution. Especially, the performance becomes much worse when three observations are utilized and Δt is not big enough. The reason for this phenomenon is that a too small Δt with less observations leads to a large condition number matrix $\mathbf{A}_N$. A larger condition number means a small perturbation may introduce a large error to the solution of linear equations. Thus, more than three observations should be used and the observation period should not be too small for the IROD problem.

Figure 5 shows the results of the Case 2 with a fixed final time, i.e., $T_f = 6000$ s. It can be seen that more observations do mean a smaller estimate error covariance but not a smaller estimate error. More observations smaller covariance is easily to understand, because this is the essential characteristic of least square method. And the reason for the trend of estimate error mean is on the relative motion dynamics. By comparing subfigure (a) with (b), it can be figured out that the case using of TH equations leads to a much better performance than the case using CW equations. Moreover, the error mean shows a decreasing trend with the increasing of the number of observations.

4.5 IROD performance analysis

In this section, Monte Carlo simulations will be conducted to further evaluate the performance of the IROD algorithm proposed in this paper and to compare it with the prototype algorithm presented in Ref. [19]. Three specific simulation cases will be examined with one parameter changed each time: Case 1, observation period $T_f = 6000$ s, initial separation

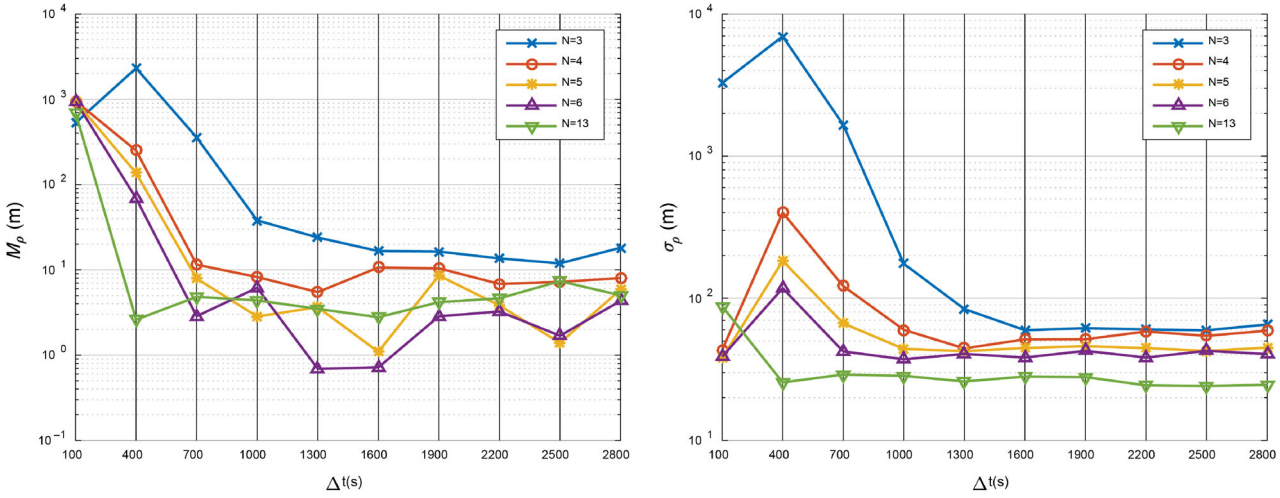

(a) CW dynamics based

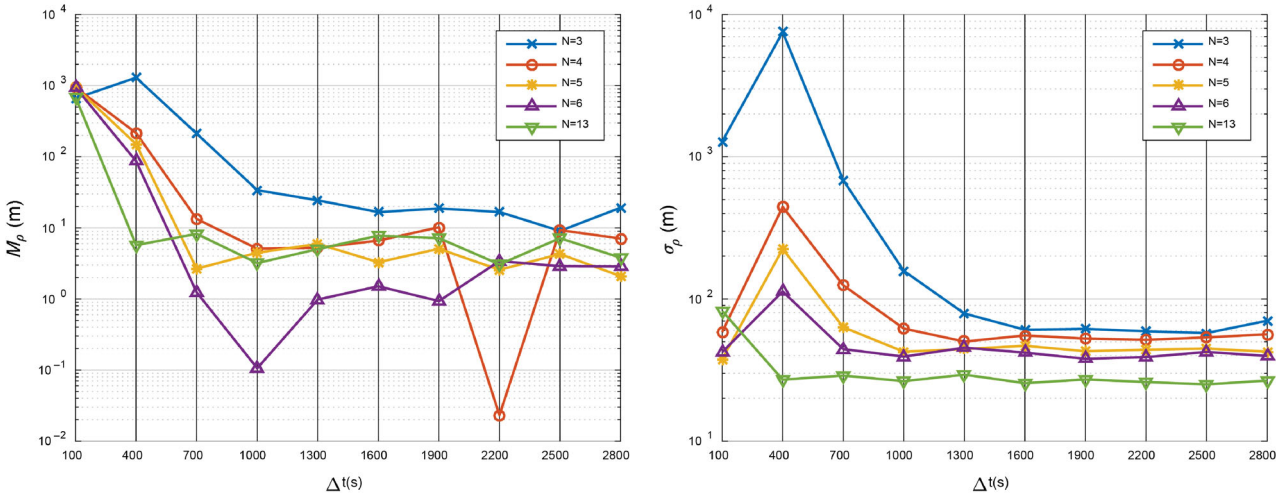

(b) TH dynamics based

Fig. 4 Estimation error mean and standard deviation, V-bar stationary, final time increases, $R_0 \approx 1000$ m.

$R_0 \approx 1000$ m; Case 2, 3000 s, 1000 m; Case 3, 6000 s, 100 m. Other parameters were provided in Table 1. Figs. 6–8 present the range estimate error mean and standard deviation for Cases 1–3, respectively, where subfigures (a) show the results for CW dynamics and the prototype algorithm in Ref. [19], subfigures (b) depict the results for CW dynamics and the proposed algorithm in this paper, and subfigures (c) describe the results for TH dynamics and proposed algorithm.

Firstly, performance improvement can be seen from the subfigures (a) and (b) of Figs. 6–8. The estimate error standard deviation based on the prototype algorithm does not always decrease as the number of observations increases, but the results of the proposed algorithm in this paper generally decrease. The reason is that these two algorithms solve the initial relative state in a different way. The prototype IROD algorithm is based on a least squares approach designed to minimize the estimate error of the scale factors $\tilde{K}$, but not the initial state x_0. In contrast, state augmentation IROD algorithm proposed in this paper is designed to minimize the estimate error of both $\tilde{K}$ and x_0 at the same time. Anyway, state augmentation means a larger state dimension which leads to a much more computational burden and the computational burden will be geometrically increased as the number of dimension linearly increases. However, IROD is not real-time navigation problem and the

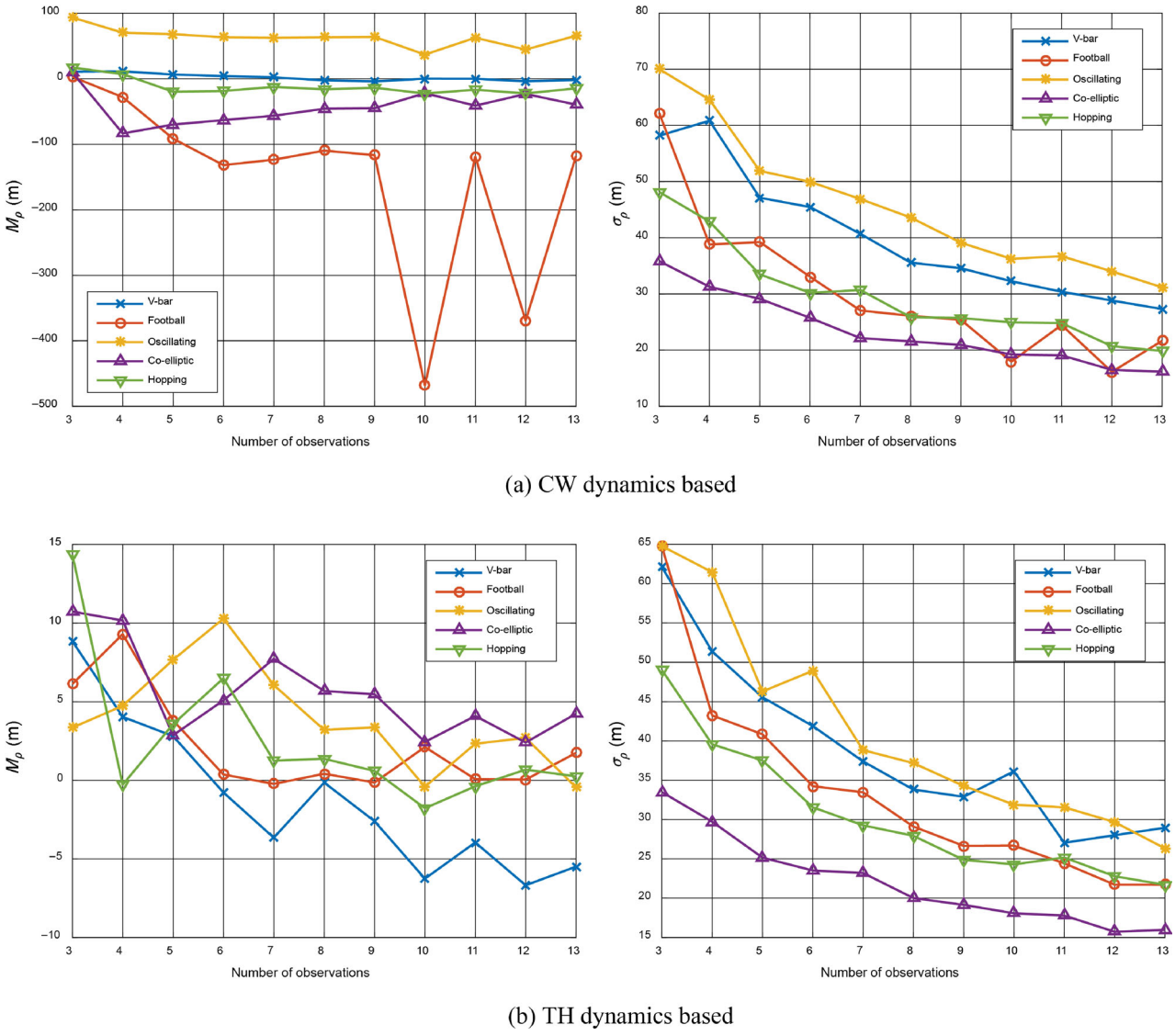

Fig. 5 Estimation error mean and standard deviation, $T_f = 6000$ s, $R_0 \approx 1000$ m.

purpose of IROD is to obtain initial relative orbit and the corresponding covariance to initialize the real-time navigation filter. Additionally, certain recursive algorithm could be used to achieve better computation efficiency [27]. Thus, the computational amount increasing to some extent should be OK for most cases.

Interestingly, as shown in the subfigures (a) and subfigures (b), they share similar performance for the case of three observations. Actually, these two algorithms are equivalent to each other when there are only three observations. Because the prototype algorithm uses all the observations to calculate $\tilde{K}$ but only the first three elements of $\tilde{K}$ are utilized to compute x_0, which lost information from other observations. As a result, these two algorithms are equivalent when there are only three observations, but the algorithm presented in this paper will achieve a better solution when there have been more measurements.

Secondly, as shown in subfigures (c), the estimated error mean are much smaller than those shown in subfigures (a) and subfigures (b). The reason is obvious since TH equations are second order dynamics, more accurate than CW equations. Anyway, there are still more accurate dynamics [28,29] than TH equations, but relevant state transition matrices need to be obtained before these improved dynamics can be used. IROD performance would be absolutely improved when high-order dynamics is used.

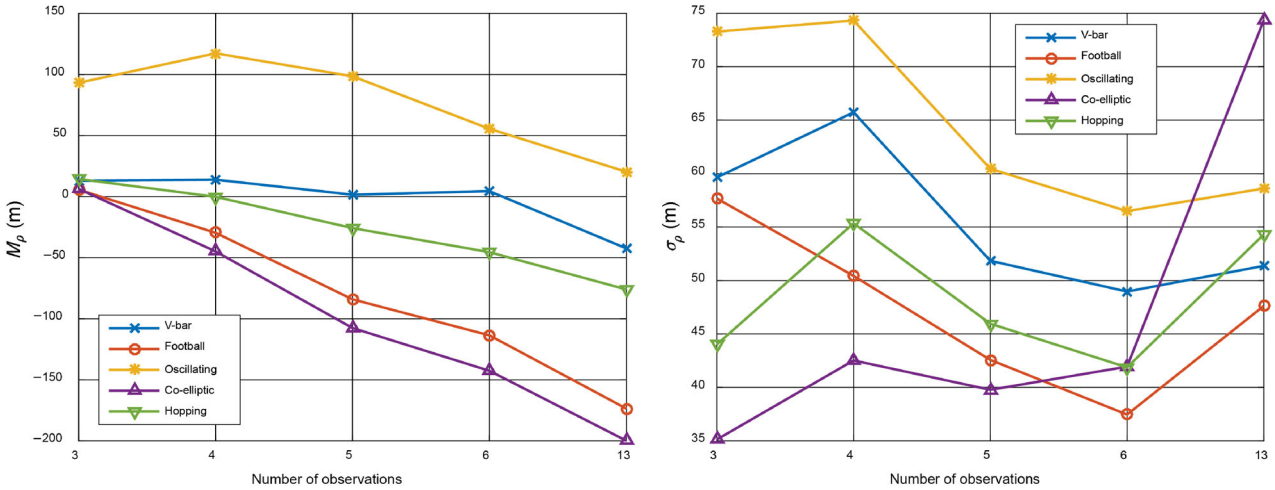

(a) Results of prototype algorithm, CW dynamics based

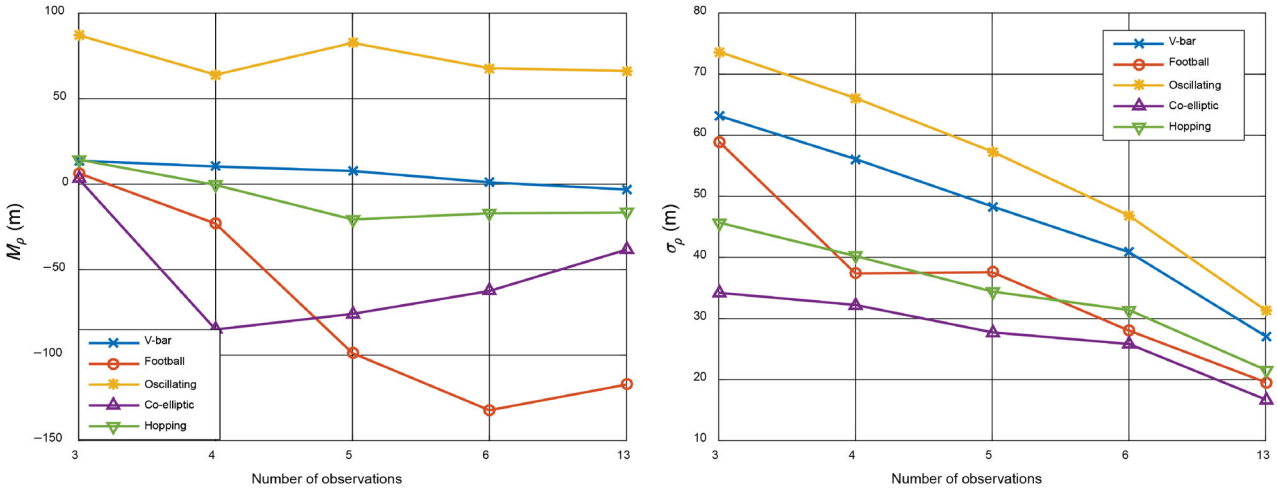

(b) Results of proposed algorithm, CW dynamics based

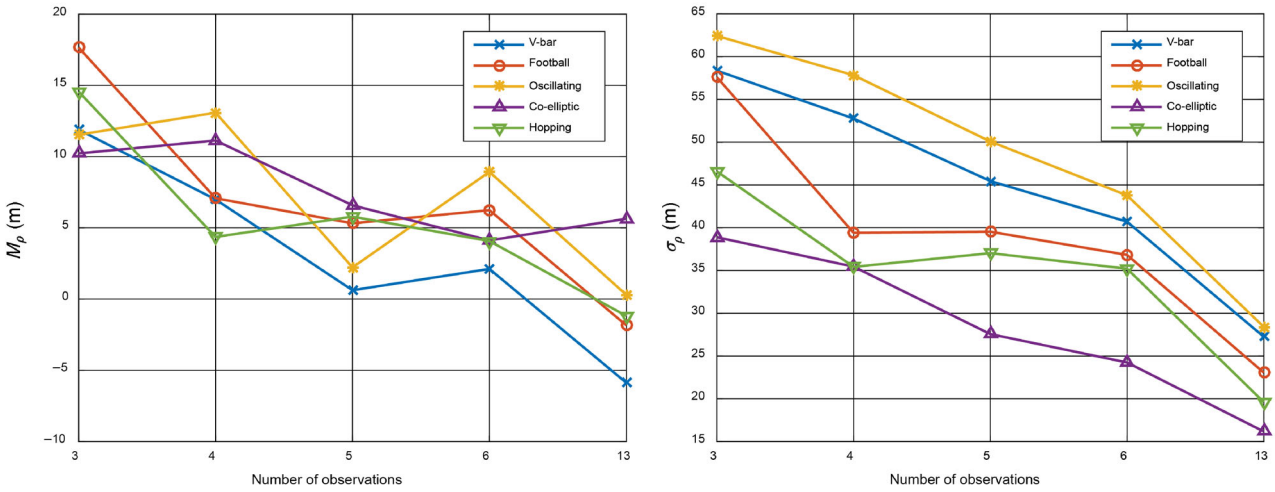

(c) Results of proposed algorithm, TH dynamics based

Fig. 6 Estimation error mean and standard deviation of Case 1.

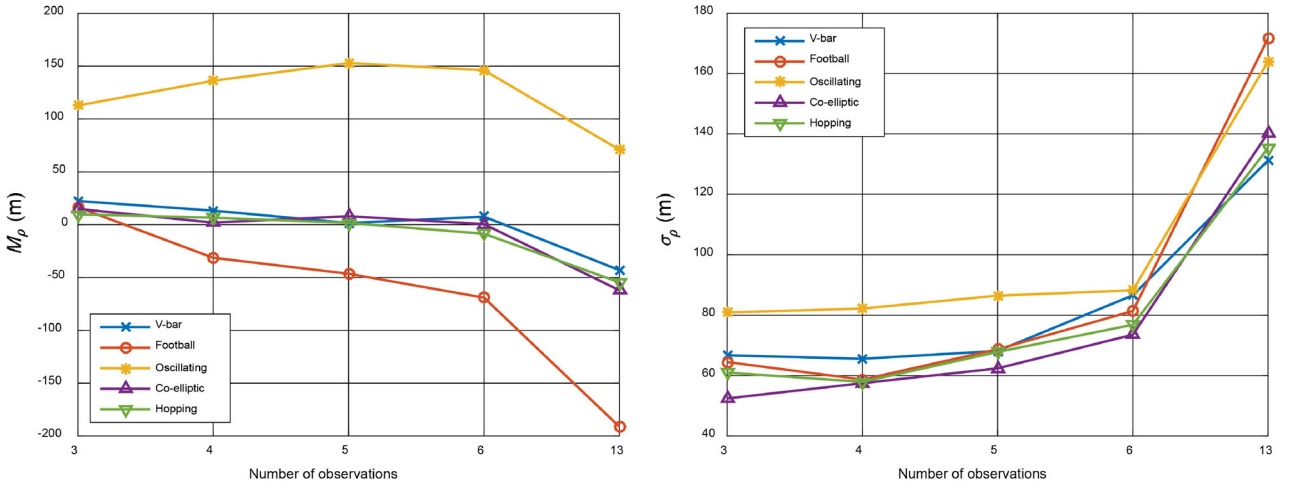

(a) Results of prototype algorithm, CW dynamics based

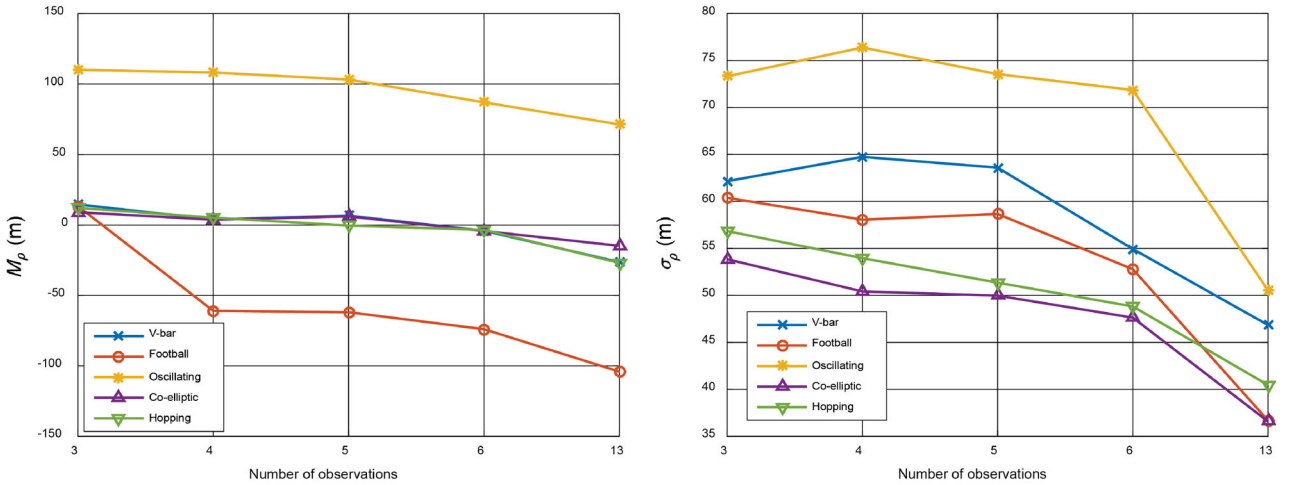

(b) Results of proposed algorithm, CW dynamics based

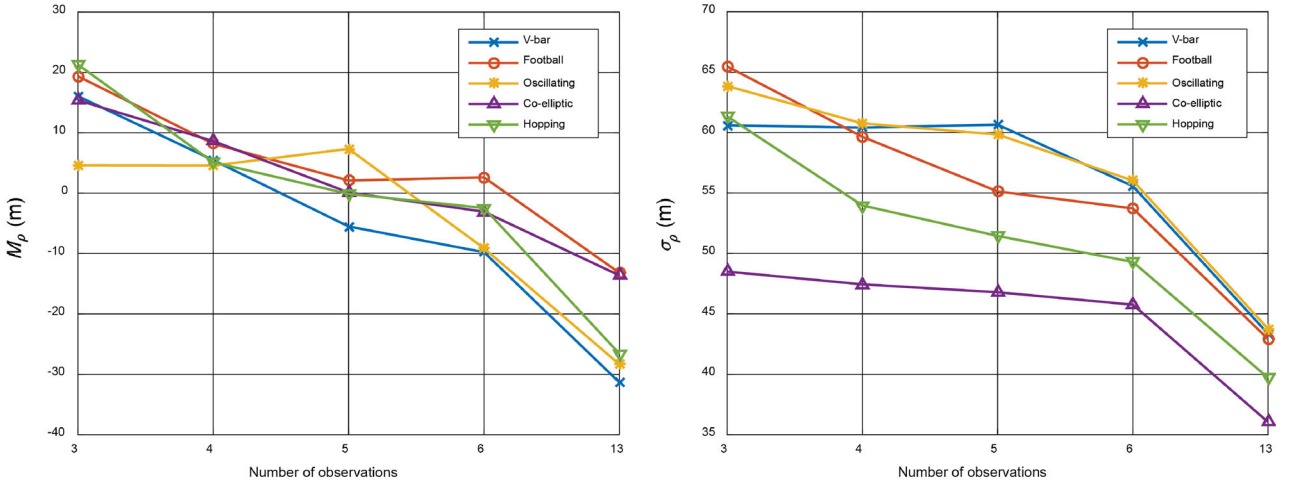

(c) Results of proposed algorithm, TH dynamics based

Fig. 7 Estimation error mean and standard deviation of Case 2.

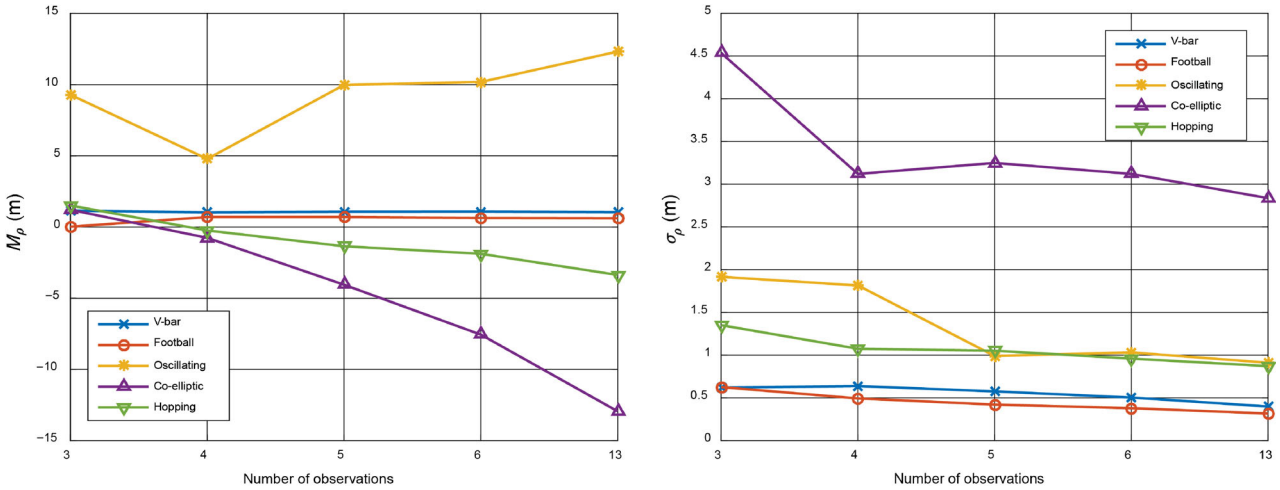

(a) Results of prototype algorithm, CW dynamics based

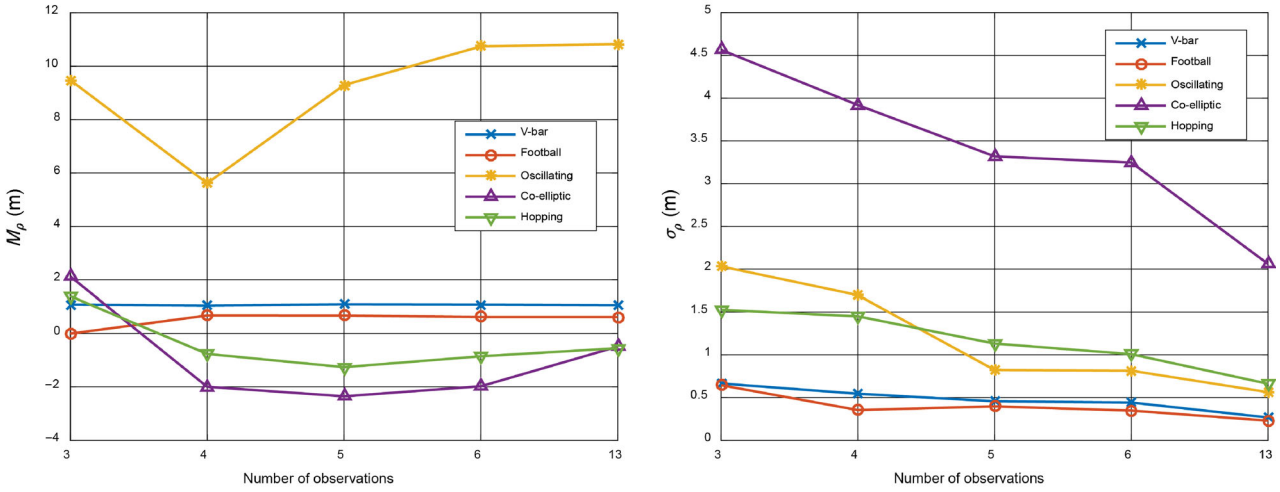

(b) Results of proposed algorithm, CW dynamics based

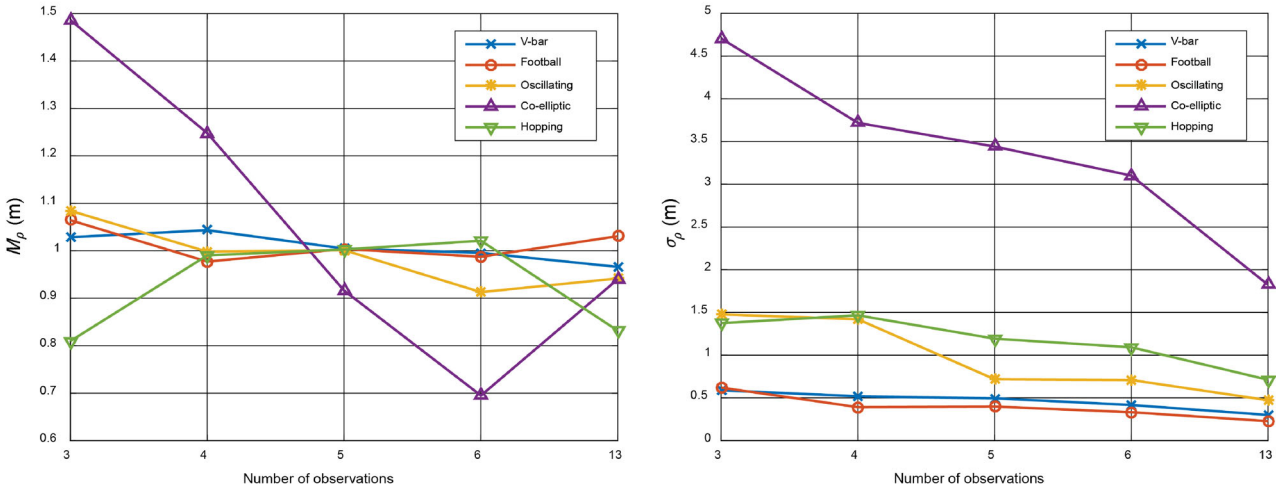

(c) Results of proposed algorithm, TH dynamics based

Fig. 8 Estimation error mean and standard deviation of Case 3.

5 Conclusions

This paper presented a global optimal least square angles-only IROD algorithm for non-cooperative spacecraft proximity operations based on the idea firstly proposed by Geller that camera offset from the chaser center-of-mass provides range observability. The state transition matrices of linearized relative motion Clohessy–Wiltshire dynamics and Tschauner–Hempel dynamics were used to establish a state augmentation least square scheme to solve the IROD problem. Additionally, the approximate analytic expressions for the estimate error mean and covariance were developed. A detailed performance analysis based on nonlinear Monte Carlo simulations for the proposed algorithms was conducted and presented. Performance was shown to be improved with the proposed algorithm in this paper, higher-order dynamics and smaller initial separation. This was also shown to be valid for a couple of relative trajectories.

Above all, an optimal angles-only initial relative orbit determination algorithm in the sense of lease square is presented and verified. The proposed algorithm generally achieves a better solution and can be used to initialize real-time navigation filter for non-cooperative spacecraft proximity operations.

Acknowledgements

The authors would like to thank Dr. David Geller from Utah State University for his great help in making this work possible. And this work is supported in part by the National Postdoctoral Program for Innovative Talents (No. BX201700304), the Foundation of Science and Technology on Aerospace Flight Dynamics Laboratory (No. 61422100306707).

References

[1] Gaias, G., D'Amico, S., Ardaens, J. S. Angles-only navigation to a non-cooperative satellite using relative orbital elements. *Journal of Guidance, Control, and Dynamics,* **2014**, 37(2): 439–451.

[2] D'Amico, S., Ardaens, J., Gaias, G., Benninghoff, H., Schlepp, B., Jorgensen, J.L. Noncooperative rendezvous using angles-only optical navigation: system design and fight results. *Journal of Guidance, Control and Dynamics,* **2013**, 36(6): 1576–1595.

[3] Eberle, S., Ohndorf, A., Faller, R. On-orbit servicing mission operations at GSOC. In: Proceedings of the SpaceOps 2010 Conference, **2010**: AIAA 2010–1975.

[4] Barnhart, D., Sullivan, B. Hunter, R., Bruhn, J., Lowler, E., Hoag, L. Phoenix project status 2013. In: Proceedings of the AIAA SPACE 2013 Conference and Exposition, **2013**.

[5] Woffinden, D., Geller, D. Observability criteria for angles-only navigation. *IEEE Transactions on Aerospace and Electronic Systems,* **2009**, 45(3): 1194–1208.

[6] Woffinden, D., Geller, D. Optimal orbital rendezvous maneuvering for angles-only navigation. *Journal of Guidance, Control, and Dynamics,* **2009**, 32(4): 1382–1387.

[7] Li, J. R., Li, H. Y., Tang, G. J., Luo, Y. Z. Research on the strategy of angles-only relative navigation for autonomous rendezvous. *Science China Technological Sciences,* **2011**, 54(7): 1865–1872.

[8] Grzymisch, J., Ficher, W. Observability criteria and unobservable maneuvers for in-orbit bearings-only navigation. *Journal of Guidance, Control, and Dynamics,* **2014**, 37(4): 1250–1259.

[9] Luo, J., Gong, B., Yuan, J., Zhang, Z. Angles-only relative navigation and closed-loop guidance for spacecraft proximity operations. *Acta Astronautica,* **2016**, 128: 91–106.

[10] Jagat, A., Sinclair, A. Control of spacecraft relative motion using angles-only navigation. In: Proceedings of the AAS/AIAA Space Flight Machanics Meeting, **2015**.

[11] Newman, B., Lovell, A., Pratt, E. Second order nonlinear initial orbit determination for relative motion using volterra theory. *Advances in the Astronautical Sciences,* **2014**, 152:1253–1272.

[12] Newman, B., Lovell, A., Pratt, E., Duncan, E. Quadratic hexa-dimensional solution for relative orbit determination. In: Proceedings of the AIAA/AAS Astrodynamics Specialist Conference, **2014**.

[13] Sullivan, J., Koenig, A., D'Amico, S. Improved maneuver-free approach to angles-only navigation for space rendezvous. In: AAS/AIAA Space Flight Mechanics Meeting, **2016**.

[14] Gasbarri, P., Sabatini, M., Palmerini, G. B. Ground tests for vision based determination and control of formation flying spacecraft trajectories. *Acta Astronautica,* **2014**, 102: 378–391.

[15] Chen, T., Xu, S. Double line-of-sight measuring relative navigation for spacecraft autonomous rendezvous. *Acta Astronautica,* **2010**, 67: 122–134.

[16] Gao, X. H., Liang, B., Pan, L. and Du, X. D. Distributed relative navigation of GEO non-cooperative target based on multiple line-of-sight measurements. *Journal of Astronautics,* **2015**, 36(3): 292–299.
[17] Klein, I., Geller, D. Zero Δv solution to the angles-only range observability problem during orbital proximity operations. *Advances in Estimation, Navigation, and Spacecraft Control,* **2012**, Springer Berlin Heidelberg, **2015**: 351–369..
[18] Geller, D., Klein, I. Angles-only navigation state observability during orbital proximity operations. *Journal of Guidance, Control, and Dynamics,* **2014**, 37(6): 1976–1983.
[19] Geller D, Perez A. Initial relative orbit determination for close-in proximity operations. *Journal of Guidance, Control, and Dynamics,* **2015**, 38(9): 1833–1842.
[20] Gong, B., Geller, D., Luo, J. Initial relative orbit determination analytical covariance and performance analysis for proximity operations. *Journal of Spacecraft and Rockets,* **2016**, 53(5): 822–835.
[21] Tschauner, J., Hempel, P. Rendezvous zu einem in elliptischer bahn umlaufenden ziel. *Astronautica Acta,* **1965**, 11(2): 104–109.
[22] Yamanaka, K., Ankersen, F. New state transition matrix for relative motion on an arbitrary elliptical orbit. *Journal of Guidance, Control, and Dynamics,* **2002**, 25(1): 60–66.
[23] Clohessy, W. H., Wiltshire, R. S. Terminal guidance system for satellite rendezvous. *Journal of the Aero/Space Sciences,* **1960**, 27(9): 653–658.
[24] Kaplan, M. H. *Modern spacecraft dynamics and control*. New York: John Wiley & Sons, Inc.: New York **1976**: 343–370.
[25] Woffinden, D. C. Angles-only navigation for autonomous orbital rendezvous. Ph.D. Dissertation. Utah State University, **2008**.
[26] Buckland, S. T. Monte Carlo confidence intervals. *Biometrics*, **1984**, 40(3): 811–817.
[27] Reali, F., Palmerini, G. Estimate problems for satellite clusters. In: Proceedings of the IEEE Aerospace Conference, **2008**.
[28] Sengupta, P., Vadali, S. , Alfriend, K. Second-order state transition for relative motion near perturbed, elliptic orbits. *Celestial Mechanics and Dynamical Astronomy,* **2007**, 97(2): 101–129.
[29] Carter, T., Humi, M. Clohessy–Wiltshire Equations Modified to Include Quadratic Drag. *Journal of Guidance, Control and Dynamics,* **2002**, 25(6): 1058–1065.

Baichun Gong is an assistant professor of Nanjing University of Aeronautics and Astronautics. He received his Ph.D. degree from the Department of Aerospace Engineering at Northwestern Polytechnical University, China, in 2016, and was a visiting scholar of the Department of Mechanical and Aerospace Engineering at Utah State University, in 2014 and 2015. Currently, he is a winner of the "National Postdoctoral Program for Innovative Talents". His area of expertise is in the aerospace flight dynamics, control and navigation for on-orbit servicing mission. His current research interests are angles-only and range-only relative navigation, and control for space rendezvous and docking. E-mail: baichun.gong@nuaa.edu.cn.

Wendan Li received her B.S. degree in aircraft design from the Department of Aeronautical Engineering at Zhengzhou University of Aeronautics, China, in 2016. She is currently pursuing her M.S. degree in aerospace engineering at Nanjing University of Aeronautics and Astronautics. She has won the first prize at the 9th China Trajectory Optimization Competition. Her research interests include angles-only relative navigation and guidance, and optimal orbit control. E-mail: lwd19950421@163.com.

Shuang Li received his B.S.E., M.S.E., and Ph.D. degrees from the Department of Aerospace Engineering at Harbin Institute of Technology, China, in 2001, 2003, and 2007, respectively. Since 2007, he has been with the College of Astronautics, Nanjing University of Aeronautics and Astronautics, China, where he is a full professor now. He was also a visiting scholar of the Department of Mechanical and Aerospace Engineering at the University of Strathclyde, UK, from 2012 to 2013. He has been the author of over 60 articles in reputable journals and conference proceedings. His research interests include spacecraft dynamics and control, deep space exploration, spacecraft autonomous guidance navigation and control, and astrodynamics. He has undertaken and is conducting up to 20 projects sponsored from the China government and the aerospace enterprises in the fields above. E-mail: lishuang@nuaa.edu.cn.

Weihua Ma received his B.S.E., M.S.E., and Ph.D. degrees from the Department of Aerospace Engineering at Northwestern Polytechnical University (NPU), China, in 2000, 2003, and 2007, respectively. Since 2007, he has been with the College of Astronautics, NPU, China, where he is an associate professor now. He was also a visiting scholar of the Department of Mechanical and Aerospace Engineering at the University of Strathclyde, UK, from 2014 to 2015. His research interests include spacecraft dynamics and control, spacecraft autonomous guidance navigation and control. He has undertaken and is conducting up to 20 projects sponsored from China government and the aerospace enterprises in the fields above. E-mail: whma_npu@nwpu.edu.cn.

Lili Zheng received her Ph.D. degrees from the Department of Aerospace Engineering at Northwestern Polytechnical University, China, in 2011. Since 2011, she has been with the Beijing Institute of Aerospace System Engineering, China, where she is a senior engineer now. Her research interests include spacecraft dynamics and control, navigation and control. E-mail: gainlyzheng@163.com.